Second harmonic generation in amorphous silicon-on-silica metamaterial

Jie Xu[1], Eric Plum[1,a)], Vassili Savinov[1], and Nikolay I. Zheludev[1,2]

1. Optoelectronics Research Centre and Centre for Photonic Metamaterials, University of Southampton, Southampton, SO17 1BJ, United Kingdom
2. Centre for Disruptive Photonic Technologies, SPMS, TPI, Nanyang Technological University, Singapore, 637371, Singapore

[a)]Author to whom correspondence should be addressed: erp@orc.soton.ac.uk

ABSTRACT

We demonstrate second harmonic generation by an amorphous silicon metamaterial fabricated on the tip of an optical fibre that collects the generated light. The metamaterial is a double chevron array that supports a closed-mode resonance for the fundamental wavelength at 1510 nm with a quality factor of 30. The normalized resonant second harmonic conversion efficiency calculated per intensity and square of interaction length is ~10^{-11}/W which exceeds the previously achieved value for silicon metamaterial by two orders of magnitude.

I. INTRODUCTION

Second-order nonlinear optical processes are of considerable importance for laser technologies, quantum optics, materials characterization, spectroscopy and imaging. Over the last decade, a substantial effort has been focused on developing plasmonic[1-8] and dielectric[9-12] metamaterials[13] with large nonlinearities for second harmonic generation (SHG). In particular, in silicon-based photonics second-order optical nonlinearities are required in various information processing schemes[14,15]. In silicon, second-order optical nonlinearity can be imposed by strain, electric field and interfaces and has been observed in waveguides[16-22], nanoparticles[23], nanowires[24,25] , nanopillars[26], photonic crystal nanocavities[27], metamaterials[28-30] and multi-material stacks with silicon[31,32]. Silicon metasurfaces have also been used to enhance the nonlinear response of materials with strong natural second-order nonlinearity[33,34]. Here we report a fibre-integrated metamaterial manufactured from amorphous silicon that achieves two orders of magnitude higher normalized conversion efficiency than previous silicon metamaterial[28].

II. SILICON METAMATERIAL ON A FIBRE TIP

The all-dielectric metamaterial reported here supports a resonant response at wavelength λ_0=1.5 μm. It is an array of chevron groove pairs, with unit cell dimensions of 1.1 × 1.0 μm^2, milled into the core of a silica fibre and subsequently coated with a 90-nm-thick amorphous silicon layer, see Fig. 1. The metamaterial geometry was chosen by considering that SHG normal to a two-dimensional structure – that is pumped at normal incidence – is permitted for structures with either three-fold or absent rotational symmetry [35,36], while resonant enhancement of SHG may be expected from Fano resonances that occur in pairs of slightly different resonators [37]. A chevron – two identical lines forming an angle – is arguably the simplest structure lacking rotational symmetry. Chevrons can be easily fabricated and combined into a compact unit cell that is smaller than its resonant wavelength. The point symmetry group of the metamaterial is D_1 (see Fig. 1b,c), limiting the allowed components of the second-order nonlinear susceptibility tensor to: $\chi^{(2)}_{yyy}$, $\chi^{(2)}_{yxx}$, $\chi^{(2)}_{xxy} = \chi^{(2)}_{xyx}$, where the first index indicates the polarization of the second harmonic photon and the other indices indicate the polarizations of the pump photons.

Within the double-V unit cell, the V-elements are of different size for the structure to support an anti-symmetric Fano-type closed mode at 1.5 μm wavelength (Fig. 1d) coupled to free-space radiation with linear polarization oriented along its symmetry axis[37-40] (*y*-axis in Fig. 1c). The metamaterial has been manufactured on the tip of a cleaved silica optical fibre (Thorlabs SM980-5.8-125, single mode at pump wavelengths) that collects and guides light transmitted or radiated by the metamaterial, see Fig. 1a,b. The fibre's numerical aperture of 0.13 implies that only the 0^{th}-order diffraction of generated second harmonic radiation will be collected. During fabrication, to reduce gallium deposits[40], the fibre tip is first coated with a thin layer of gold and then the V-shaped groves are created by milling with a focused gallium ion beam through the gold layer to the depth of about 256 nm into silica. After removing the sacrificial gold layer, a 90-nm layer of amorphous silicon is deposited by plasma enhanced chemical vapour deposition on the entire patterned fibre tip. The metamaterial covers the entire core of the fibre, which has a nominal diameter of 10 μm. The metamaterial's thickness, from the lowest point of the silicon layer at the bottom of the chevron grooves to its highest point at the silicon/air interface in between the chevron pairs, is L=346 nm.

The metamaterial's transmission spectra were modelled (Comsol Multiphysics 5.4) assuming a plane wave normally incident onto a unit cell with periodic boundary conditions, Fig. 1d. The simulations assume a real refractive index of 1.44 for glass and the complex refractive index of the silicon layer according to ellipsometry measurements on an unstructured area (Supplementary Figure S1). The structure's transmission spectra were measured by illuminating the fibre tip with normally incident linearly polarized white light and detecting the transmitted light with an optical spectrum analyser (Ando AQ-6315E), using an unstructured cleaved fibre without the silicon film as a reference, Fig. 1e. Experimental and modelled transmission spectra of the metamaterial are in qualitative agreement. The closed-mode resonance is seen at a wavelength of 1.5 μm, only under *y*-polarized illumination (along the symmetry axis; see Fig. 1c). According to our simulations, the electric field at the silicon interfaces is up to 8× larger than the incident field (Supplementary Figure S2). The experimentally observed quality factor of this resonance is about 30, calculated by $Q=\lambda_0/\Delta\lambda$, where λ_0=1.5 μm is the resonance's central wavelength and $\Delta\lambda$ is the resonance's full width at half maximum (FWHM). Compared with the modelling, the measured resonance is wider due to fabrication-related residual contamination with gallium and inhomogeneous broadening (i.e. slight variations in sizes of key features across different unit cells).

III. SECOND HARMONIC GENERATION

Considering that second harmonic generation by unstructured interfaces vanishes at normal incidence[41] and in order to detect second harmonic generation caused by the metamaterial structure, we measure SHG with a normally incident pump beam, which also ensures that 0^{th} order SHG diffraction is within the acceptance angle of the optical fibre. The second-harmonic response of the metamaterial was characterized in the pump wavelength range from 1440 nm to 1610 nm with linearly polarized 200 fs optical pulses of up to 35 mW average power (~9 GW/cm^2 peak intensity) and 80 MHz repetition rate from an optical parametric oscillator (Spectra Physics Inspire HF 100). Transmitted pump light was filtered out. As control experiments, the same nonlinear measurements were conducted with a bare fibre tip and on a tip of fibre covered by an unstructured 90-nm-thick layer of CVD-silicon. Strong second harmonic emission is observed only for *y*-polarized pump light at 1510 nm wavelength with the metamaterial-bearing fibre, Fig. 2a, while control experiments detected no second harmonic above the noise level. The second harmonic nature of the signal is confirmed by its dependence on the average pump power at 1510 nm wavelength, see Fig. 2b. The second harmonic spectral

peak coincides with the metamaterial's absorption resonance, as expected from microscopic theory of second harmonic generation[42].

2.9 pW second harmonic power (P_{SH}) has been observed for 35 mW y-polarized average pump power (P_{pump}), corresponding to a second harmonic generation power conversion efficiency of at least $\eta=P_{SH}/P_{pump}=0.8\times10^{-10}$, which is comparable with efficiencies in metallic structures[43,44] and exceeds previously reported silicon metamaterial by four orders of magnitude[28]. We note that the fibre's refractive index of about 1.45 implies that some diffraction will occur into the fibre at free-space wavelengths shorter than 1.6 μm, while diffraction into air occurs at wavelengths shorter than 1.1 μm. The fibre's numerical aperture of 0.13 implies that only radiation propagating close to normal to the metamaterial will be collected. Therefore, the calculated efficiency of our structure only accounts for 0th order diffraction of SHG into the fibre. Diffraction of SHG up to the 1st order into air and up to the 2nd order into glass implies that the metamaterial's true SHG efficiency may be a few times higher. To allow comparison with other materials, we need to consider that phase-matched – sufficiently thin films are always phase matched – SH conversion efficiency increases linearly with pump peak intensity I and quadratically with interaction length L=346 nm. Therefore we arrive at a normalized efficiency of $\eta/(IL^2)= 8\times10^{-3}$/GW corresponding to $\chi^{(2)}_{yyy}$~0.3 pm/V, which is comparable to KDP[45]. The normalized efficiency reported here exceeds previous silicon metamaterial[28] by two orders of magnitude. This improvement is largely due to resonant enhancement of second harmonic generation at the closed-mode resonance of the double chevron structure.

According to symmetry analysis[46], this metamaterial – and any other 2D structure of D_1 symmetry with symmetry axis y – has three allowed components of the second-order susceptibility: $\chi^{(2)}_{yyy}$, $\chi^{(2)}_{yxx}$ and $\chi^{(2)}_{xyx}=\chi^{(2)}_{xxy}$. However, second harmonic detection through the standard single-mode fibre, that hosts the nonlinear metamaterial and does not maintain polarization, does not allow direct polarization measurements on the generated second harmonic light. In order to probe the relative strengths of the allowed susceptibility tensor components, second harmonic power was detected with left-circularly, right-circularly and linearly polarized pump light at several orientations relative to metamaterial's symmetry axis. The inset in Fig. 2b shows generated second harmonic power as a function of the azimuth of the linear pump polarization at 1510 nm pump wavelength. The second-order susceptibility tensor components were extracted by fitting the pump-polarization-dependent intensity of generated second harmonic signal giving $\left|x^{(2)}_{xyx}/x^{(2)}_{yyy}\right|=0.2$ and $\left|x^{(2)}_{yxx}/x^{(2)}_{yyy}\right|=0.2$ at this resonant wavelength. $\chi^{(2)}_{yyy}$ is the dominant susceptibility tensor component. More details are provided in Supplementary Section S1.

Beyond symmetry considerations and the observed Fano resonance, we note that the structure may also support guided modes within the metamaterial layer[47,48], which could play a role in coupling resonators and SHG. Furthermore, while diffraction above the 0th order will not be guided by the fibre and thus cannot contribute directly to the detected SHG, it could affect the conversion efficiency indirectly.

Our results show how pumping at an anti-symmetric Fano-type resonance of a structure lacking inversion symmetry yields substantial second harmonic generation in an amorphous silicon metamaterial. We believe that the second-order nonlinearity can be increased further by increasing the Q-factor of this resonance and by engineering a second resonance at the SHG wavelength. This may be achieved by adjusting the metamaterial design, more accurate nanofabrication (to avoid inhomogeneous broadening) and by avoiding gallium ion implantation during nanofabrication (e.g. by using electron beam lithography or imprint techniques).

VI. CONCLUSIONS

In summary, we have demonstrated second harmonic generation in amorphous silicon metamaterial with a power conversion efficiency of ~10^{-10}, an efficiency improvement of four orders of magnitude over previous silicon metamaterials. This improvement is achieved by exploiting the double-chevron structure's closed-mode resonance. Our findings demonstrate how mesoscopic structuring – that combines closed-mode resonances with a suitable choice of point group symmetry – enables the fabrication of metamaterials with quadratic optical nonlinearity from amorphous dielectrics. Second harmonic generation by the double-chevron metamaterial of D_1 symmetry is most efficient for pump light polarized along its symmetry axis and all allowed net second-order nonlinear susceptibility tensor components have been determined. Ease of deposition of amorphous materials shall enable the fabrication of nonlinear elements of nanoscale thickness on complex non-planar platforms, such as end-facets of optical fibres and silicon photonics waveguides.

SUPPLEMENTARY MATERIAL

See the supplementary material for the complex refractive index of the silicon layer, the metamaterial's modelled electric field enhancement at the silicon interfaces and details of the nonlinear tensor characterization.

ACKNOWLEDGEMENTS

This work is supported by the UK's Engineering and Physical Sciences Research Council (grant EP/M009122/1), Singapore A*STAR QTE program (SERC A1685b0005), Singapore Ministry of Education (grant MOE2016-T3-1-006 (S)) and Chinese Scholarship Council (CSC No. 201706310145).

DATA AVAILABILITY

Following a period of embargo, the data from this paper will be available from the University of Southampton ePrints research repository: https://doi.org/10.5258/SOTON/D1626

REFERENCES

[1] J. Butet, P. F. Brevet, and O. J. F. Martin, "Optical second harmonic generation in plasmonic nanostructures: from fundamental principles to advanced applications," ACS Nano **9**, 10545-10562 (2015). doi: 10.1021/acsnano.5b04373.

[2] R. Czaplicki, A. Kiviniemi, M. J. Huttunen, X. Zang, T. Stolt, I. Vartiainen, J. Butet, M. Kuittinen, O. J. F. Martin, and M. Kauranen, "Less is more: enhancement of second-harmonic generation from metasurfaces by reduced nanoparticle density," Nano Letters **18**, 7709-7714 (2018). doi: 10.1021/acs.nanolett.8b03378.

[3] S. D. Gennaro, M. Rahmani, V. Giannini, H. Aouani, T. P. H. Sidiropoulos, M. Navarro-Cía, S. A. Maier, and R. F. Oulton, "The interplay of symmetry and scattering phase in second harmonic generation from gold nanoantennas," Nano Letters **16**, 5278-5285 (2016). doi: 10.1021/acs.nanolett.6b02485.

[4] Y. B. Habibullah, K. Iwata, and T. Ishihara, "Second-harmonic generation from complementary Au metasurfaces with triangular resonators," Journal of the Optical Society of America B-Optical Physics **36**, 1166-1175 (2019). doi: 10.1364/Josab.36.001166.

[5] J. Lee, M. Tymchenko, C. Argyropoulos, P. Y. Chen, F. Lu, F. Demmerle, G. Boehm, M.-C. Amann, A. Alù, and M. A. Belkin, "Giant nonlinear response from plasmonic metasurfaces coupled to intersubband transitions," Nature **511**, 65-69 (2014). doi: 10.1038/nature13455.

[6] N. Nookala, J. Lee, M. Tymchenko, J. S. Gomez-Diaz, F. Demmerle, G. Boehm, K. Lai, G. Shvets, M. C. Amann, A. Alu, and M. Belkin, "Ultrathin gradient nonlinear metasurface with a giant nonlinear response," Optica **3**, 283-288 (2016). doi: 10.1364/OPTICA.3.000283.
[7] N. C. Panoiu, W. E. I. Sha, D. Y. Lei, and G. C. Li, "Nonlinear optics in plasmonic nanostructures," Journal of Optics **20**, 083001 (2018). doi: 10.1088/2040-8986/aac8ed.
[8] T. Chang, S. Jeon, M. Heo, and J. Shin, "Mimicking bio-mechanical principles in photonic metamaterials for giant broadband nonlinearity," Commun. Phys. **3**, 79 (2020). doi: 10.1038/s42005-020-0352-0.
[9] S. Liu, M. B. Sinclair, S. Saravi, G. A. Keeler, Y. Yang, J. Reno, G. M. Peake, F. Setzpfandt, I. Staude, T. Pertsch, and I. Brener, "Resonantly enhanced second-harmonic generation using III–V semiconductor all-dielectric metasurfaces," Nano Letters **16**, 5426-5432 (2016). doi: 10.1021/acs.nanolett.6b01816.
[10] F. J. F. Lochner, A. N. Fedotova, S. Liu, G. A. Keeler, G. M. Peake, S. Saravi, M. R. Shcherbakov, S. Burger, A. A. Fedyanin, I. Brener, T. Pertsch, F. Setzpfandt, and I. Staude, "Polarization-dependent second harmonic diffraction from resonant GaAs metasurfaces," Acs Photonics **5**, 1786-1793 (2018). doi: 10.1021/acsphotonics.7b01533.
[11] P. P. Vabishchevich, S. Liu, M. B. Sinclair, G. A. Keeler, G. M. Peake, and I. Brener, "Enhanced second-harmonic generation using broken symmetry III–V semiconductor Fano metasurfaces," ACS Photonics **5**, 1685-1690 (2018). doi: 10.1021/acsphotonics.7b01478.
[12] I. Volkovskaya, L. Xu, L. Huang, A. I. Smirnov, A. E. Miroshnichenko, and D. Smirnova, "Multipolar second-harmonic generation from high-Q quasi-BIC states in subwavelength resonators," Nanophotonics **9**, 3953-3963 (2020). doi: 10.1515/nanoph-2020-0156.
[13] A. E. Minovich, A. E. Miroshnichenko, A. Y. Bykov, T. V. Murzina, D. N. Neshev, and Y. S. Kivshar, "Functional and nonlinear optical metasurfaces," Laser & Photonics Reviews **9**, 195-213 (2015). doi: 10.1002/lpor.201400402.
[14] C. Langrock, S. Kumar, J. E. McGeehan, A. E. Willner, and M. M. Fejer, "All-optical signal processing using $\chi^{(2)}$ nonlinearities in guided-wave devices," Journal of Lightwave Technology **24**, 2579-2592 (2006). doi: 10.1109/JLT.2006.874605.
[15] A. E. Willner, A. Fallahpour, F. Alishahi, Y. Cao, A. Mohajerin-Ariaei, A. Almaiman, P. Liao, K. Zou, A. N. Willner, and M. Tur, "All-optical signal processing techniques for flexible networks," Journal of Lightwave Technology **37**, 21-35 (2019). doi: 10.1109/JLT.2018.2873245.
[16] L. Alloatti, D. Korn, C. Weimann, C. Koos, W. Freude, and J. Leuthold, "Second-order nonlinear silicon-organic hybrid waveguides," Optics Express **20**, 20506-20515 (2012). doi: 10.1364/oe.20.020506.
[17] I. Avrutsky and R. Soref, "Phase-matched sum frequency generation in strained silicon waveguides using their second-order nonlinear optical susceptibility," Optics Express **19**, 21707-21716 (2011). doi: 10.1364/OE.19.021707.
[18] M. Cazzanelli, F. Bianco, E. Borga, G. Pucker, M. Ghulinyan, E. Degoli, E. Luppi, V. Véniard, S. Ossicini, D. Modotto, S. Wabnitz, R. Pierobon, and L. Pavesi, "Second-harmonic generation in silicon waveguides strained by silicon nitride," Nature Materials **11**, 148-154 (2012). doi: 10.1038/nmat3200.
[19] N. K. Hon, K. K. Tsia, D. R. Solli, and B. Jalali, "Periodically poled silicon," Applied Physics Letters **94**, 091116 (2009). doi: 10.1063/1.3094750.
[20] R. S. Jacobsen, K. N. Andersen, P. I. Borel, J. Fage-Pedersen, L. H. Frandsen, O. Hansen, M. Kristensen, A. V. Lavrinenko, G. Moulin, H. Ou, C. Peucheret, B. Zsigri, and A. Bjarklev, "Strained silicon as a new electro-optic material," Nature **441**, 199-202 (2006). doi: 10.1038/nature04706.
[21] A. Rao and S. Fathpour, "Second-harmonic generation in integrated photonics on silicon," Physica Status Solidi (a) **215**, 1700684 (2018). doi: 10.1002/pssa.201700684.

[22] C. Castellan, A. Trenti, C. Vecchi, A. Marchesini, M. Mancinelli, M. Ghulinyan, G. Pucker, and L. Pavesi, "On the origin of second harmonic generation in silicon waveguides with silicon nitride cladding," Scientific Reports **9**, 1088 (2019). doi: 10.1038/s41598-018-37660-x.
[23] S. V. Makarov, M. I. Petrov, U. Zywietz, V. Milichko, D. Zuev, N. Lopanitsyna, A. Kuksin, I. Mukhin, G. Zograf, E. Ubyivovk, D. A. Smirnova, S. Starikov, B. N. Chichkov, and Y. S. Kivshar, "Efficient second-harmonic generation in nanocrystalline silicon nanoparticles," Nano Letters **17**, 3047-3053 (2017). doi: 10.1021/acs.nanolett.7b00392.
[24] M. Khorasaninejad, M. A. Swillam, K. Pillai, and S. S. Saini, "Silicon nanowire arrays with enhanced optical properties," Optics Letters **37**, 4194-4196 (2012). doi: 10.1364/OL.37.004194.
[25] P. R. Wiecha, A. Arbouet, H. Kallel, P. Periwal, T. Baron, and V. Paillard, "Enhanced nonlinear optical response from individual silicon nanowires," Physical Review B **91**, 121416 (2015). doi: 10.1103/PhysRevB.91.121416.
[26] B. Dev Choudhury, P. K. Sahoo, R. Sanatinia, G. Andler, S. Anand, and M. Swillo, "Surface second harmonic generation from silicon pillar arrays with strong geometrical dependence," Optics Letters **40**, 2072-2075 (2015). doi: 10.1364/OL.40.002072.
[27] M. Galli, D. Gerace, K. Welna, T. F. Krauss, L. O'Faolain, G. Guizzetti, and L. C. Andreani, "Low-power continuous-wave generation of visible harmonics in silicon photonic crystal nanocavities " Opt. Express **18**, 26613-26624 (2010). doi: 10.1364/OE.18.026613.
[28] J. Bar-David and U. Levy, "Nonlinear diffraction in asymmetric dielectric metasurfaces," Nano Letters **19**, 1044-1051 (2019). doi: 10.1021/acs.nanolett.8b04342.
[29] Y. Q. An and A. C. Diebold, "Transiently stimulated second-harmonic generation from silicon nanogratings," Physical Review B **96**, 201306 (2017). doi: 10.1103/PhysRevB.96.201306.
[30] K. T. Lee, M. Taghinejad, J. Yan, A. S. Kim, L. Raju, D. K. Brown, and W. Cai, "Electrically biased silicon metasurfaces with magnetic Mie resonance for tunable harmonic generation of light," ACS Photonics **6**, 2663-2670 (2019). doi: 10.1021/acsphotonics.9b01398.
[31] H. H. Lin, M. H. Yang, R. Sharma, M. W. Puckett, S. Montoya, C. D. Wurm, F. Vallini, E. E. Fullerton, and Y. Fainman, "Synthesis of second-order nonlinearities in dielectric-semiconductor-dielectric metamaterials," Applied Physics Letters **110**, 113103 (2017). doi: 10.1063/1.4978640.
[32] H. H. Lin, F. Vallini, M. H. Yang, R. Sharma, M. W. Puckett, S. Montoya, C. D. Wurm, E. E. Fullerton, and Y. Fainman, "Electronic metamaterials with tunable second-order optical nonlinearities," Scientific Reports **7**, 9983 (2017). doi: 10.1038/s41598-017-10304-2.
[33] N. Bernhardt, K. Koshelev, S. J. U. White, K. W. C. Meng, J. E. Fröch, S. Kim, T. T. Tran, D. Y. Choi, Y. Kivshar, and A. S. Solntsev, "Quasi-BIC resonant enhancement of second-harmonic generation in WS_2 monolayers," Nano Letters **20**, 5309-5314 (2020). doi: 10.1021/acs.nanolett.0c01603.
[34] Q. Yuan, L. Fang, H. Fang, J. Li, T. Wang, W. Jie, J. Zhao, and X. Gan, "Second harmonic and sum-frequency generations from a silicon metasurface integrated with a two-dimensional material," ACS Photonics **6**, 2252-2259 (2019). doi: 10.1021/acsphotonics.9b00553.
[35] S. Bhagavantam and P. Chandrasekhar, "Harmonic generation and selection rules in nonlinear optics," Proceedings of the Indian Academy of Sciences - Section A **76**, 13-20 (1972). doi: 10.1007/BF03048332.
[36] K. Konishi, T. Higuchi, J. Li, J. Larsson, S. Ishii, and M. Kuwata-Gonokami, "Polarization-controlled circular second-harmonic generation from metal hole arrays with threefold rotational symmetry," Physical Review Letters **112**, 135502 (2014). doi: 10.1103/PhysRevLett.112.135502.

[37] V. A. Fedotov, M. Rose, S. L. Prosvirnin, N. Papasimakis, and N. I. Zheludev, "Sharp trapped-mode resonances in planar metamaterials with a broken structural symmetry," Physical Review Letters **99**, 147401 (2007). doi: 10.1103/PhysRevLett.99.147401.
[38] B. Luk'yanchuk, N. I. Zheludev, S. A. Maier, N. J. Halas, P. Nordlander, H. Giessen, and C. T. Chong, "The Fano resonance in plasmonic nanostructures and metamaterials," Nature Materials **9**, 707-715 (2010). doi: 10.1038/nmat2810.
[39] S. Campione, S. Liu, L. I. Basilio, L. K. Warne, W. L. Langston, T. S. Luk, J. R. Wendt, J. L. Reno, G. A. Keeler, I. Brener, and M. B. Sinclair, "Broken symmetry dielectric resonators for high quality factor Fano metasurfaces," ACS Photonics **3**, 2362-2367 (2016). doi: 10.1021/acsphotonics.6b00556.
[40] V. Savinov and N. I. Zheludev, "High-quality metamaterial dispersive grating on the facet of an optical fiber," Applied Physics Letters **111**, 091106 (2017). doi: 10.1063/1.4990766.
[41] N. Bloembergen, R. K. Chang, and C. H. Lee, "Second-harmonic generation of light in reflection from media with inversion symmetry," Physical Review Letters **16**, 986-989 (1966). doi: 10.1103/PhysRevLett.16.986.
[42] K. O'Brien, H. Suchowski, J. Rho, A. Salandrino, B. Kante, X. Yin, and X. Zhang, "Predicting nonlinear properties of metamaterials from the linear response," Nat. Mater. **14**, 379-383 (2015). doi: 10.1038/nmat4214.
[43] S. Keren-Zur, O. Avayu, L. Michaeli, and T. Ellenbogen, "Nonlinear beam shaping with plasmonic metasurfaces," ACS Photonics **3**, 117-123 (2016). doi: 10.1021/acsphotonics.5b00528.
[44] N. Segal, S. Keren-Zur, N. Hendler, and T. Ellenbogen, "Controlling light with metamaterial-based nonlinear photonic crystals," Nature Photonics **9**, 180-184 (2015). doi: 10.1038/Nphoton.2015.17.
[45] R. W. Boyd, *Nonlinear optics*, 3rd ed. (Academic Press, Burlington, MA, 2008).
[46] S. Popov, Y. P. Svirko, and N. I. Zheludev, *Susceptibility tensors for nonlinear optics*. (CRC Press, 1995).
[47] M. Gould, A. Pomerene, C. Hill, S. Ocheltree, Y. Zhang, T. Baehr-Jones, and M. Hochberg, "Ultra-thin silicon-on-insulator strip waveguides and mode couplers," Appl. Phys. Lett. **101**, 221106 (2012). doi: 10.1063/1.4768296.
[48] Z. Zou, L. Zhou, X. Li, and J. Chen, "60-nm-thick basic photonic components and bragg gratings on the silicon-on-insulator platform," Opt. Express **23**, 20784-20795 (2015). doi: 10.1364/OE.23.020784.

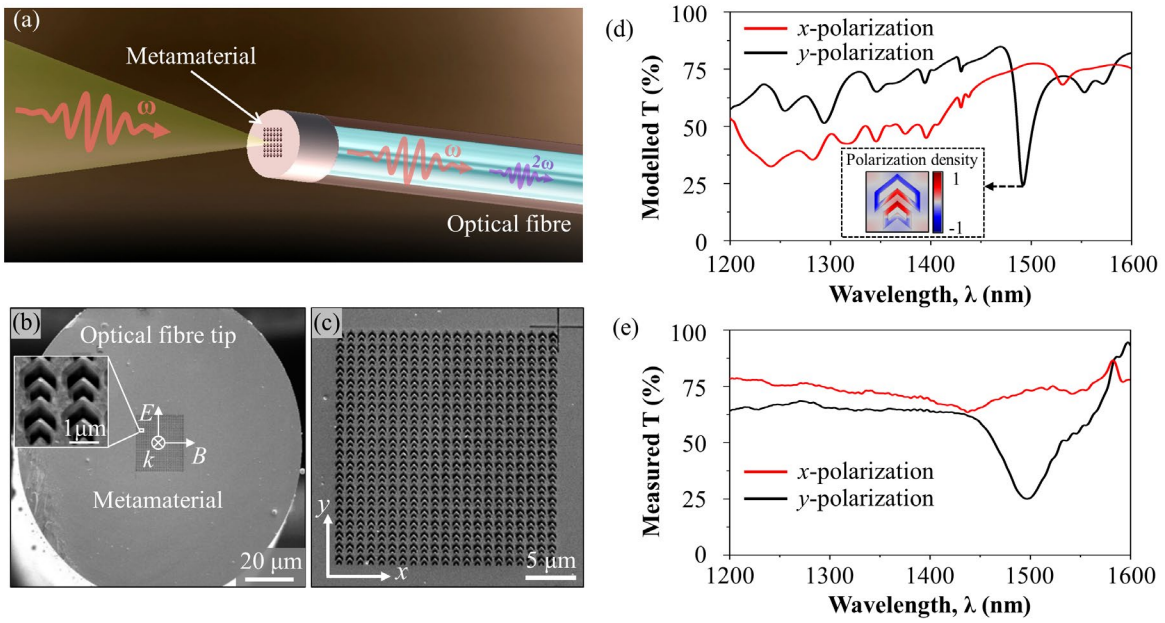

Figure 1: Nonlinear silicon metamaterial on a fibre tip. (a) Artistic impression of the experimental characterization of the metamaterial's nonlinearity. (b) SEM image of the nonlinear metamaterial fabricated on the end-facet of a single-mode optical fibre. The metamaterial covers the core of a cleaved optical fibre and consists of pairs of chevron grooves in silica, coated with an amorphous silicon layer. Inset: magnified view of a metamaterial section. (c) Magnified view of the entire metamaterial. (To prevent charging, SEM imaging took place with an additional gold coating that was subsequently removed.) (d) Modelled and (e) measured linear transmission spectra of the metamaterial as a function of wavelength for *x* (red) and *y* (black) polarization. The inset in (d) shows the *y* component of the linear polarization density distribution at the resonance.

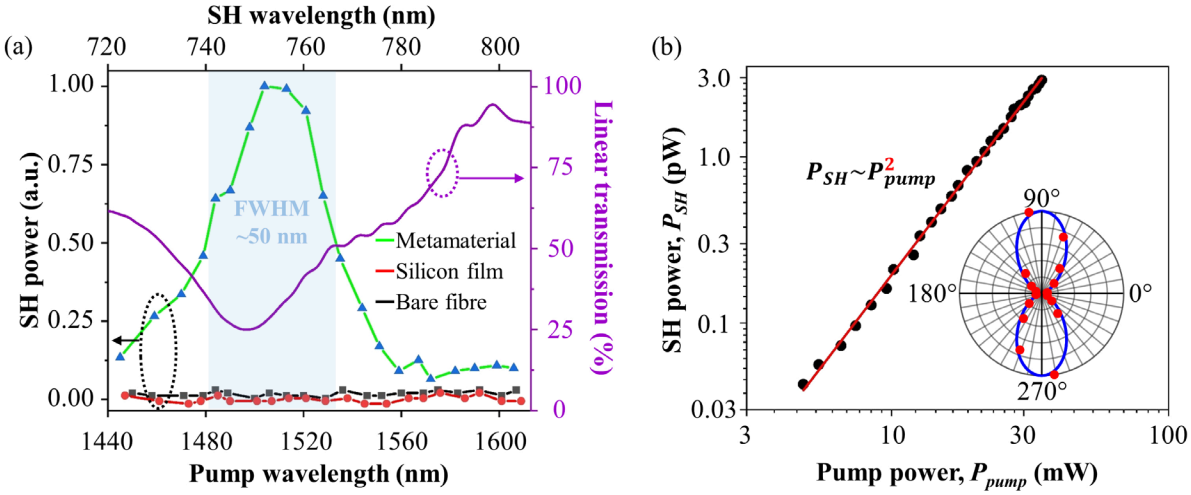

Figure 2: Observation of second harmonic generation. (a) Detected spectral dependence of second harmonic (SH) emission by metamaterial on a cleaved fibre (green), unstructured silicon film on a cleaved fibre (red) and an unstructured bare cleaved fibre (black) alongside the metamaterial's linear transmission spectrum (purple) for *y*-polarized pump light. (b) Power dependence of second harmonic generation by the metamaterial (black dots) with a quadratic fit (red curve) at 1510 nm pump wavelength for *y*-polarized pump light. The inset shows the generated second harmonic power as a function of the azimuth of the linear pump polarization at 1510 nm pump wavelength (the resonance). Dots indicate measurements and the blue curve shows a fit.

Supplementary Information: Second harmonic generation in amorphous silicon-on-silica metamaterial

Jie Xu[1], Eric Plum[1], Vassili Savinov[1], and Nikolay I. Zheludev[1,2]

[1] Optoelectronics Research Centre and Centre for Photonic Metamaterials, University of Southampton, Southampton, SO17 1BJ, United Kingdom
[2] Centre for Disruptive Photonic Technologies, SPMS, TPI, Nanyang Technological University, Singapore, 637371, Singapore

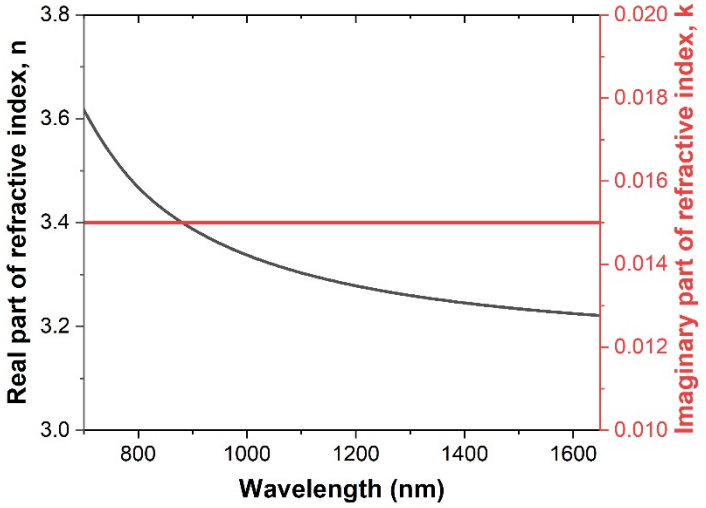

Figure S1. Refractive index of the fabricated amorphous silicon thin film according to ellipsometry measurements on an unstructured area.

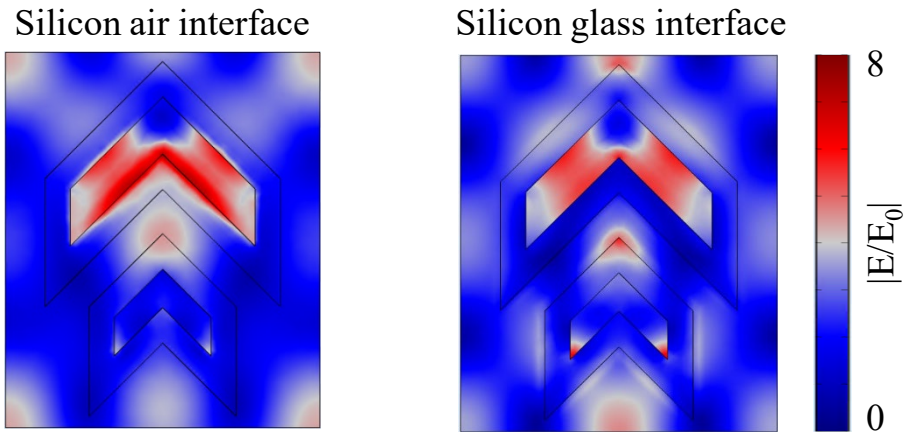

Figure S2. Electric field enhancement at the silicon interfaces relative to the amplitude $|E_0|$ of the incident wave, for the case of a normally incident *y*-polarized wave at the 1.5 μm wavelength resonance.

S1. $\chi^{(2)}$ tensor characterization

S1.1 Pump field

The incident field that drives the metamaterial is given by:

$E(t) = \alpha\sqrt{P_{pump}} \cdot (\hat{x}\cos\theta + \hat{y}\sin\theta\, e^{i\phi})e^{i\omega t}$	S1.1

Electric field and incident power P_{pump} are linked by a proportionality constant α, $|E(t)|^2 = \alpha^2 P_{pump}$. The angle ϕ determines the polarization ellipticity of the incident light. In case of linearly polarized light (ϕ=0), θ is the polarization azimuth measured relative to the *x*-axis. The *y*-polarization (ϕ=0, θ=90°) is along the symmetry axis of the metamaterial, see Fig. S3. Left and right circularly polarized pump light is given by ϕ=±90° and θ=45°.

The observable field is given by the real part of the previous expression:

$E_{obs}(t) = Re\big(E(t)\big) = \alpha\sqrt{P_{pump}} \cdot (\hat{x}\cos\theta\cos\omega t + \hat{y}\sin\theta\cos(\phi + \omega t))$	S1.2

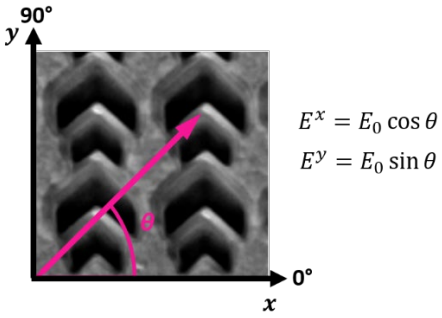

Figure S3. Schematic of linearly polarized (ϕ=0) **pump laser light** of azimuth θ incident on the metamaterial with symmetry axis *y*.

S1.2 SHG intensity

Assuming the metamaterial has D_1 symmetry with symmetry axis along *y*, the allowed second order nonlinear susceptibility tensor components are: $\chi^{(2)}_{xxy} = \chi^{(2)}_{xyx}, \chi^{(2)}_{yxx}, \chi^{(2)}_{yyy}$, where the first index indicates the second harmonic polarization and the latter indices indicate the polarization of the pump photons.

It is convenient to parametrized them as:

$\chi^{(2)}_{xyx} = \chi^{(2)}_{xxy} = ae^{i\gamma}\chi^{(2)}_{yyy}$	S1.3
$\chi^{(2)}_{yxx} = be^{i\varphi}\chi^{(2)}_{yyy}$	S1.4

Where $a = |\boldsymbol{x}^{(2)}_{xyx}/\boldsymbol{x}^{(2)}_{yyy}|$, $b = |\boldsymbol{x}^{(2)}_{yxx}/\boldsymbol{x}^{(2)}_{yyy}|$ are real-valued and non-negative. The second harmonic field is then (using Eq. S1.1 and dropping α and $e^{i2\omega t}$ in the second step for simplicity):

$E_{SH} \propto \left(\chi^{(2)}_{xyx} + \chi^{(2)}_{xxy}\right)E_xE_y \cdot \hat{x} + \left(\chi^{(2)}_{yxx}E_xE_x + \chi^{(2)}_{yyy}E_yE_y\right)\cdot\hat{y}$ $\propto \chi^{(2)}_{yyy}P_{pump} \cdot \{2a\cos\theta\sin\theta \cdot e^{i(\phi+\gamma)} \cdot \hat{x} + (b\cos^2\theta e^{i\varphi} + \sin^2\theta e^{i2\phi}) \cdot \hat{y}\}$	S1.5

The total second harmonic power is given by the sum of the *x*- and *y*-polarized second harmonic powers:

$$P_{SH} = P_{SH}^{x} + P_{SH}^{y} \propto |E_{SH}^{x}|^2 + \left|E_{SH}^{y}\right|^2 \propto \left|\chi_{yyy}^{(2)}\right|^2 P_{pump}^2 \cdot \{4a^2\cos^2\theta\sin^2\theta + b^2\cos^4\theta + \sin^4\theta + 2b\cos^2\theta\sin^2\theta\cos(\varphi - 2\phi)\} \quad \text{S1.6}$$

At this point we drop $\left|\chi_{yyy}^{(2)}\right|^2$ and write this in terms of second harmonic photon counts $N(\theta, \phi, P_{pump})$, which correspond to the difference between the detected counts $N_D(\theta, \phi, P_{pump})$ and the detector's dark-counts, N_{dark} that we assume to be constant. Important special cases are listed in Table S1.

$$N(\theta, \phi, P_{pump}) = N_D(\theta, \phi, P_{pump}) - N_{dark} \propto P_{pump}^2 \cdot \{4a^2\cos^2\theta\sin^2\theta + \sin^4\theta + b^2\cos^4\theta + 2b\cos^2\theta\sin^2\theta\cos(\varphi - 2\phi)\} \quad \text{S1.7}$$

Pump polarization	**Second harmonic photon counts**, $N(\theta, \phi, P_{pump})$
Circular ϕ=±90°, ϑ=45°	$P_{pump}^2 \cdot \{a^2 + \frac{1}{4} + \frac{1}{4}b^2 - \frac{1}{2}b\cos(\varphi)\}$
Diagonal linear ϕ=0°, ϑ=45° or 135°	$P_{pump}^2 \cdot \{a^2 + \frac{1}{4} + \frac{1}{4}b^2 + \frac{1}{2}b\cos(\varphi)\}$
x-polarization ϕ=0°, ϑ=0°	$P_{pump}^2 \cdot \{b^2\}$
y-polarization ϕ=0°, ϑ=90°	$P_{pump}^2 \cdot \{1\}$

Table S1. Second harmonic photon counts for selected pump polarizations according to Eq. S1.7.

S1.3 Linear and circular polarization experiments

For linear pump polarization (ϕ=0°) at fixed pump power P_{pump}, the pump azimuth (θ) dependence of second harmonic photon counts relative to the case of *y*-polarized pumping is given by:

$$\frac{N(\theta, 0, P_{pump})}{N(90°, 0, P_{pump})} = \frac{N_D(\theta, 0, P_{pump}) - N_{dark}}{N_D(90°, 0, P_{pump}) - N_{dark}} = 4a^2\cos^2\theta\sin^2\theta + \sin^4\theta + b^2\cos^4\theta + 2b\cos^2\theta\sin^2\theta\cos(\varphi) \quad \text{S1.8}$$

The second harmonic photon counts as a function of the linear polarization angle θ of the excitation laser were measured at five pump wavelengths and fitted by Eq. S1.8. Brute-force lookup of all the possible values for $a = \left|x_{xyx}^{(2)}/x_{yyy}^{(2)}\right|$, $b = \left|x_{yxx}^{(2)}/x_{yyy}^{(2)}\right|$, and $\varphi = \arg\chi_{yxx}^{(2)} - \arg\chi_{yyy}^{(2)}$ constrains the nonlinear susceptibility tensor components that are consistent with the experiments. The range of possible solutions is shown by Fig. S4. $\left|x_{yxx}^{(2)}/x_{yyy}^{(2)}\right|$ is well-constrained at each pumping wavelength, see panel a. However, experiments with only linear pump polarization yield a range of solutions for $\left|x_{xyx}^{(2)}/x_{yyy}^{(2)}\right|$ and $\cos\varphi$. To break this ambiguity and fully characterize the susceptibility tensor components of our metamaterial, we further measured second harmonic generation with circularly polarized excitation at 1510 nm pump wavelength, where the second harmonic

generation is strongest. The measurements, that were conducted at an average power of 12 mW, reveal $\left|x_{xyx}^{(2)}/x_{yyy}^{(2)}\right|$ =0.2, $\left|x_{yxx}^{(2)}/x_{yyy}^{(2)}\right| = 0.2$ and φ=±83° at a pump wavelength of 1510 nm according to Eq. S1.7 (see also Table S1).

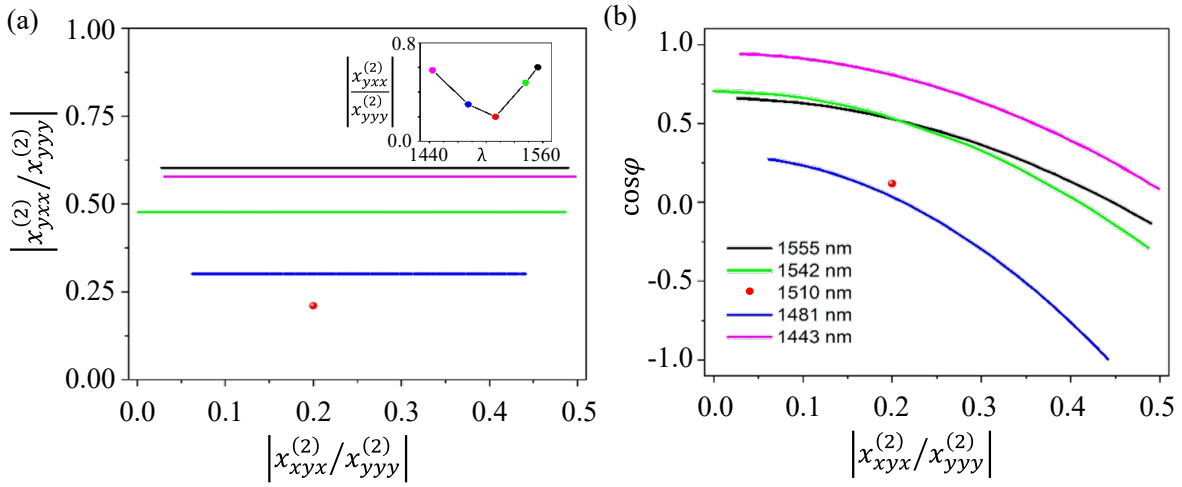

Figure S4. (a) Possible susceptibility ratios $\left|x_{yxx}^{(2)}/x_{yyy}^{(2)}\right|$ as a function of possible ratios $\left|x_{xyx}^{(2)}/x_{yyy}^{(2)}\right|$. The inset shows the dependence of the first ratio on the pump wavelength. (b) Possible values of cos φ as a function of possible ratios $\left|x_{xyx}^{(2)}/x_{yyy}^{(2)}\right|$.